

See discussions, stats, and author profiles for this publication at: <https://www.researchgate.net/publication/272081748>

# Carbonation of Wollastonite(001) Competing Hydration: Microscopic Insights from Ion Spectroscopy and Density Functional Theory

ARTICLE in ACS APPLIED MATERIALS & INTERFACES · FEBRUARY 2015

Impact Factor: 6.72 · DOI: 10.1021/am508313g · Source: PubMed

---

CITATIONS

3

---

READS

55

## 6 AUTHORS, INCLUDING:



Kyeongjae Cho

University of Texas at Dallas

302 PUBLICATIONS 9,450 CITATIONS

[SEE PROFILE](#)



Peter Thissen

Karlsruhe Institute of Technology

33 PUBLICATIONS 491 CITATIONS

[SEE PROFILE](#)

# Carbonation of Wollastonite(001) Competing Hydration: Microscopic Insights from Ion Spectroscopy and Density Functional Theory

Roberto C. Longo,<sup>†</sup> Kyeongjae Cho,<sup>†</sup> Philipp Brüner,<sup>‡</sup> Alexander Welle,<sup>§,⊥</sup> Andreas Gerdes,<sup>§</sup> and Peter Thissen<sup>\*,§</sup>

<sup>†</sup>Department of Materials Science and Engineering, University of Texas at Dallas, 800 West Campbell Road, Richardson, Texas 75080, United States

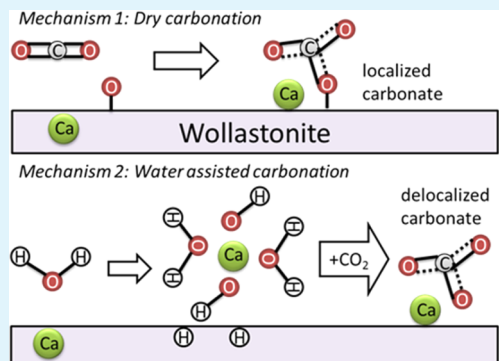
<sup>‡</sup>ION-TOF GmbH, Heisenbergstr. 15, 48149 Muenster, Germany

<sup>§</sup>Institut für Funktionelle Grenzflächen, Karlsruher Institut für Technologie, Hermann-von-Helmholtz-Platz 1, 76344 Eggenstein-Leopoldshafen, Germany

<sup>⊥</sup>Karlsruhe Nano Micro Facility, Karlsruher Institut für Technologie, Hermann-von-Helmholtz-Platz 1, 76344 Eggenstein-Leopoldshafen, Germany

**ABSTRACT:** In this paper, we report about the influence of the chemical potential of water on the carbonation reaction of wollastonite ( $\text{CaSiO}_3$ ) as a model surface of cement and concrete. Total energy calculations based on density functional theory combined with kinetic barrier predictions based on nudge elastic band method show that the exposure of the water-free wollastonite surface to  $\text{CO}_2$  results in a barrier-less carbonation.  $\text{CO}_2$  reacts with the surface oxygen and forms carbonate ( $\text{CO}_3^{2-}$ ) complexes together with a major reconstruction of the surface. The reaction comes to a standstill after one carbonate monolayer has been formed. In case one water monolayer is covering the wollastonite surface, the carbonation is no more barrier-less, yet ending in a localized monolayer. Covered with multilayers of water, the thermodynamic ground state of the wollastonite completely changes due to a metal–proton exchange reaction (also called early stage hydration) and  $\text{Ca}^{2+}$  ions are partially removed from solid phase into the  $\text{H}_2\text{O}/\text{wollastonite}$  interface. Mobile  $\text{Ca}^{2+}$  reacts again with  $\text{CO}_2$  and forms carbonate complexes, ending in a delocalized layer. By means of high-resolution time-of-flight secondary-ion mass spectrometry images, we confirm that hydration can lead to a partially delocalization of  $\text{Ca}^{2+}$  ions on wollastonite surfaces. Finally, we evaluate the impact of our model surface results by the meaning of low-energy ion-scattering spectroscopy combined with careful discussion about the competing reactions of carbonation vs hydration.

**KEYWORDS:** calcium silicate, density functional theory, time-of-flight secondary-ion mass spectrometry, low-energy ion scattering, metal–proton exchange reaction



## 1. INTRODUCTION

In 2013, there were  $\sim 0.04\%$   $\text{CO}_2$  and  $\sim 4\%$   $\text{H}_2\text{O}$  in the atmosphere of the world.<sup>1</sup> One of the consequences is that carbonate layers become ubiquitous on cement and concrete. The carbonation reaction is one of the most important processes in construction chemistry, which is in sharp contrast to the knowledge about its reaction mechanisms.

In this work, we focus on the influence of water on the carbonation reaction. This appears reasonable due to the simple fact that both components are omnipresent when the hydration of cement is started. We discuss carefully a possible competition between the carbonation and the hydration reaction, representing a possible explanation why cement stays fluid for a few hours after mixing with water.<sup>2</sup>

There is a gap in the literature in the models investigated for the carbonation reaction in context with cement. In most cases  $\text{Ca}(\text{OH})_2$  is taken as a model of the cement phase. In 2010, Montes-Hernandez et al. investigated the kinetics of carbo-

nation of solid  $\text{Ca}(\text{OH})_2$  by means of infrared spectroscopy, finding an activation of molecular water adsorbed on the solid  $\text{Ca}(\text{OH})_2$  of reacting particles.<sup>3</sup> This water activation has been quantified in an interesting density-functional theory (DFT) study by Funk and Trettin in 2013.<sup>4</sup> With the help of first-principles calculations, the difference between a water-free and a water-assisted reaction pathway was explained. Already in 2007, Black et al. underlined the importance of amorphous carbonate to be kinetically favorable over crystalline phases.<sup>5</sup>

In the first part of our paper we use first-principles calculations within DFT to predict certain reaction scenarios, placing the focus on kinetic effects of the reaction mechanism of the carbonation. While the carbonation reaction from fully water-free to dry ambient has the characteristic of building a

Received: November 26, 2014

Accepted: February 4, 2015

self-assembled monolayer, including the self-limitation character, the high influence of water on this reaction becomes clear with further rising of the chemical potential of water. In the presence of water, a metal–proton exchange reaction (MPER) is happening and leading the wollastonite surface to a nonstoichiometric thermodynamic ground state in equilibrium with a  $\text{Ca}(\text{OH})_2$  solution.<sup>6</sup> Consequently, the reaction with  $\text{CO}_2$  can take place inside the solution. To confirm our theoretical results, we extend this study in the second part by experimental results. With the help of high resolution time-of-flight secondary-ion mass spectrometry images (ToF-SIMS), we show that hydration in combination with carbonation can lead to a partially delocalization of  $\text{Ca}^{2+}$  ions on wollastonite surfaces. Finally, we evaluate the impact of our model surface results by means of low-energy ion-scattering (LEIS) spectroscopy.

## 2. METHODOLOGY

**A. Computational Details.** The calculations were performed using DFT within the generalized gradient approximation (GGA), as implemented in the Vienna ab initio simulation package.<sup>7,8</sup> The electron–ion interaction was described within the projector-augmented wave scheme.<sup>9</sup> The electronic wave functions were expanded into plane waves up to a kinetic energy of 360 eV. Wollastonite ( $\text{CaSiO}_3$ ) is a mineral formed by Ca-coordinated Si–O tetrahedra. The structure contains two apex-to-apex joining tetrahedra together with another tetrahedron with one edge parallel to the chain direction. In this work, we considered the (001) surface of wollastonite (Wol) by means of a supercell containing two layers of oxygen-terminated  $\text{Ca}_3\text{Si}_3\text{O}_9$  units and  $2 \times 2$  unit cells, for a total number of 124 atoms, plus adsorbed molecules and a vacuum region of approximately 20 Å, large enough to avoid interactions between the surface and adsorbed molecules and their replica images. In the last section, to represent the reaction of the  $\text{CO}_2$  molecule with the Wol(001) covered with more than one monolayer of  $\text{H}_2\text{O}$ , we use a cluster model to model the surface reactant:  $\text{Ca}(\text{OH})_2 + 3\text{H}_2\text{O}$ . This assumption is justified because, due to the MPER, the  $\text{Ca}^{2+}$  has been removed partially from the surface and is available for the carbonate reaction in the solution, as will be explained in detail later.

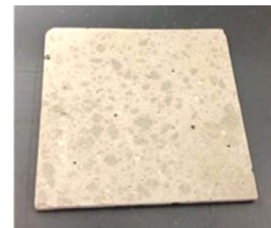
All the atoms and degrees of freedom, except the bottom Si layer, were allowed to relax via a conjugate gradient technique until the forces on the atoms were below 10 meV/Å. The Brillouin zone integration was performed using a  $4 \times 4 \times 1$  mesh within the Monkhorst–Pack scheme.<sup>10</sup> The PBE functional was used to describe the electron exchange and correlation energies within the GGA.<sup>11</sup>

The kinetic barriers were obtained with the nudged elastic band method,<sup>12,13</sup> using a string of geometric configurations (images) to describe the reaction pathways of the  $\text{CO}_2$  molecule adsorbed on the hydrated Wol(001) surface under different  $\text{H}_2\text{O}$  chemical potential conditions. A spring interaction between every configuration ensured continuity of the reaction pathway. During the relaxation, the initial and final configurations are kept frozen as the images move according to the constraint of the “elastic band”. The minimum energy path is then found when the components perpendicular to the elastic band vanish, with the relative positions of the images and the barrier being determined by the parallel components of the forces. The initial and final configurations of the different pathways were obtained by fully relaxing the Wol(001) surface

(with appropriate  $\text{H}_2\text{O}$  partial pressure conditions depending on the case under study) together with the desorbed/adsorbed  $\text{CO}_2$  molecule.

Finally, to determine whether a specific reaction must overcome a kinetic energy barrier, we performed ab initio molecular dynamics (MD) simulations at room temperature (273 K). The velocity Verlet algorithm coupled with the Nose thermostat was used to solve the equations of motion. A time step of 0.5 fs was used during an equilibration period of 10 000 steps, for a total simulation time of 5 ps.

**B. Sample Preparation.** Commercial cement (Figure 1): Commercial cement of class CEM 1 42.5 R was mixed with



Commercial Cement

Figure 1. Commercial cement of class CEM 1 42.5 R in a  $4 \times 4 \times 12$  cm prism and cut with a diamond saw to  $4 \text{ cm} \times 4 \text{ cm} \times 1 \text{ mm}$  samples.

water (0.50 water-to-cement ratio) and filled in a  $4 \times 4 \times 12$  cm prism. After the cement was cured for 2 days, samples were cut off with the help of a diamond saw ( $4 \text{ cm} \times 4 \text{ cm} \times 1 \text{ mm}$ , see Figure 1).

Wollastonite (Figure 2): A small part of this natural stone was broken mechanically. The fragment was embedded into

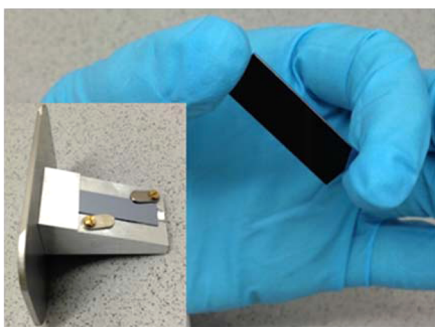


Wollastonite(001)

Figure 2. Natural wollastonite stone was broken mechanically, embedded into two-component resin and finally polished before investigation (radius of the circle 2 cm).

two-component resin (Araldite) and left for hardening for 8 h. After curing, the sample was processed on a sapphire AMT 550 grinding and polishing machine. The granularities of the individual grinding steps using SiC grinding paper were 300, 600, 1,200, 2,500, and, finally, 4,000 (200 rpm). The sample was polished with  $3 \mu\text{m}$  polycrystalline diamond suspension (150 rpm).

Ultrathin calcium silicate hydrate (C-S-H) (Figure 3): A  $3 \times 1$  cm Si(111) (FloatZone) (n-doped) crystal was chemically cleaned with a 30 min exposure at 80 °C to a 1:3 solution of aqueous  $\text{H}_2\text{O}_2$ : 18 M  $\text{H}_2\text{SO}_4$  (piranha solution). Afterward, the



### Ultrathin C-S-H Phase

**Figure 3.** An ultrathin (3 nm) calcium silicate hydrate phase was synthesized on a Si(111) wafer (size of the wafer 3 cm × 1 cm × 500 μm). Earlier investigations concerning the chemical nature of the resulting C–S–H phases have shown they are ultrathin and perfectly reproducible.

crystal was rinsed thoroughly with deionized water with a resistivity of 0.055 μS/cm. Following the cleaning, the silicon crystal was promptly mounted in a purchased closed fluid cell with tube connections, leading the fluid in a circle, which were connected with a peristaltic pump for a continuous fluid exchange, while the flow was adjusted to 500 μL/min for 12 h at room temperature. The aqueous solution of Ca(OH)<sub>2</sub> (1 mmol/L, 100 mL) was purged with Ar to avoid any effects due to CO<sub>2</sub> contamination. Earlier investigations concerning the chemical nature of the resulting C–S–H phases have shown they are ultrathin and perfectly reproducible.<sup>14</sup>

**C. Sample Characterization.** Transport of the samples was performed every time in N<sub>2</sub>-filled boxes to avoid contact with the atmosphere.

**Time-of-Flight Secondary-Ion Mass spectrometry (ToF-SIMS).** The ToF-SIMS analysis was carried out on a gridless reflectron-based ToF-SIMS V (ION-TOF GmbH, Muenster, Germany), equipped with a bismuth-cluster ion source. All spectra and images were obtained using Bi<sub>3</sub><sup>+</sup> primary ions at 25 keV energy in the high current bunched mode, with a mass resolution of  $m/\Delta m = 6000$ . The beam diameter was about 3–5 μm and all measurements were made under static conditions (primary ion dose  $< F_{PI} = 5 \times 10^{12}$  ions cm<sup>-2</sup>) on an area of 500 × 500 μm<sup>2</sup> with 256<sup>2</sup> pixels.

**Low-Energy Ion Scattering (LEIS).** LEIS measurements were done using a Qtac analyzer (ION-TOF GmbH, Münster, Germany), applying a 3.0 keV <sup>4</sup>He<sup>+</sup> beam at a beam current of 2.3 nA and a fixed scatter angle of 145°. Each measurement lasted 120 s. The fraction of backscattered He ions was measured as a function of the kinetic energy with a double toroidal analyzer, imaging the ions according to their energy onto a position-sensitive electrostatic detector. The use of this analyzer-detector combination was important because the large scatter angle of detection combined with the parallel detection increases the sensitivity by orders of magnitude and allows a reduction of the overall ion dose needed for measurements. Consequently, the total ion dose was very low compared to the surface atomic density, and therefore, ion-induced sputtering and intermixing were negligible.

## 3. RESULTS

To develop an accurate picture of the CO<sub>2</sub> adsorption process described in the Introduction, we performed DFT simulations.

First, we will describe the CO<sub>2</sub> reacting with H<sub>2</sub>O-free Wol(001) and discuss the kinetics of the chemical reaction. To study the influence of water on the kinetics of this reaction, we will stepwise increase the chemical potential of water at the Wol(001)/water interface before it reacts again with CO<sub>2</sub>.

**A. CO<sub>2</sub> Reacting with H<sub>2</sub>O-Free Wol(001).** The first scenario considered in our study is the oxygen-terminated, H<sub>2</sub>O-free Wol(001) surface. Figure 4 shows the reaction with a

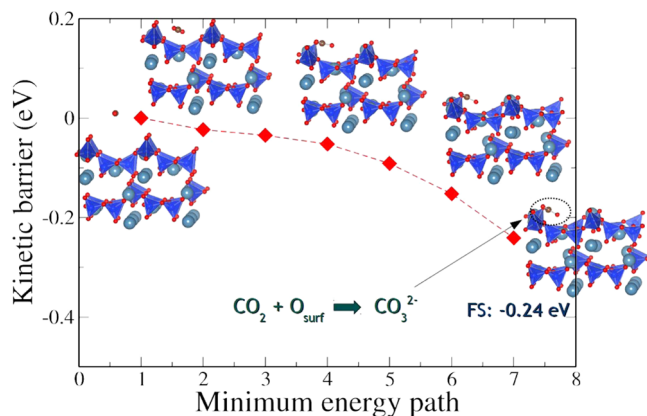


**Figure 4.** Minimum energy path of CO<sub>2</sub> reacting with water-free Wol(001). Deep blue tetrahedra represent Si atoms; red, O; light blue, Ca; and brown spheres, C atoms, respectively.

CO<sub>2</sub> molecule. The CO<sub>2</sub> undergoes a carbonate reaction with one of the tetrahedrally coordinated surface oxygen atoms to form a CO<sub>3</sub><sup>2-</sup> group. This reaction happens spontaneously without any kinetic barrier. Indeed, starting from a configuration where the CO<sub>2</sub> molecule physisorbs in the valley formed by the oxygen tetrahedra (see Figure 4), it moves along the equipotential surface energy of the valley until, after an ab initio MD simulation time of 20 ps, the CO<sub>2</sub> molecule forms the CO<sub>3</sub><sup>2-</sup> group aforementioned. Despite the absence of kinetic barrier for the carbonation of the H<sub>2</sub>O-free Wol(001) surface, we must also indicate that the binding energy is relatively low, 2.24 eV/supercell (280 meV/CaSiO<sub>3</sub> formula unit), thus indicating the ease with which the CO<sub>2</sub> could be desorbed in an annealing process. The Si–O bond is relatively strong but still slight changes can be noticed in the local structure. The volume of the Si–O tetrahedron does not change after CO<sub>2</sub> adsorption but the unsaturated Si–O bond (the one not connected to other Si–O tetrahedra) stretches after the O–C bond formation: from 1.56 to 1.64 Å. The other three Si–O bonds shorten to keep constant the volume of the tetrahedron (from 1.66 to 1.63 Å).

**B. CO<sub>2</sub> Reacting with Wol(001) Covered by a Monolayer of H<sub>2</sub>O.** The situation is remarkably different if the Wol(001) surface is covered by H<sub>2</sub>O at different coverages (chemical potential conditions); i.e., we have an OH-terminated surface. In this paragraph, we consider the two limit cases: below one H<sub>2</sub>O monolayer and a full H<sub>2</sub>O monolayer coverage. Figure 5 shows the initial and final configurations of a CO<sub>2</sub> molecule adsorbed on the OH-terminated Wol(001) surface with less than one H<sub>2</sub>O monolayer coverage. In our study, we consider both Si–OH and Ca–OH terminations. As can be seen in Figure 5, the CO<sub>2</sub> selectively reacts with the Ca–OH forming a carbonate since the Si–O bond is too strong to be broken or stretched, and only a Si–OH::O–C–O hydrogen bond is formed; see Figure

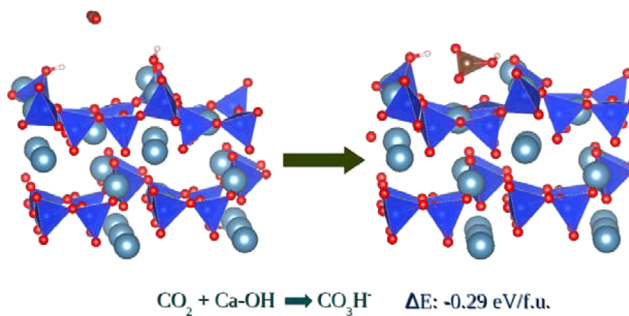


**Figure 5.** Initial and final configurations of  $\text{CO}_2$  reacting with  $\text{Wol}(001)$  covered by less than a monolayer of water. Deep blue tetrahedra represent Si atoms; red, O; light blue, Ca; white, H; and brown spheres, C atoms, respectively.

5). As a result, the Ca–O is stretched considerably (from 2.04 to 2.71 Å), finally resulting in the formation of a  $\text{CO}_3\text{H}^-$  group. The reaction energy is obviously very similar to the  $\text{H}_2\text{O}$ -free  $\text{Wol}(001)$  surface, 2.39 eV (299 meV/ $\text{CaSiO}_3$  formula unit), and it is also a spontaneous (barrier-less), exothermic process.

With full  $\text{H}_2\text{O}$  monolayer coverage (obtained after full relaxation of the  $\text{H}_2\text{O}$ -free  $\text{Wol}(001)$  surface saturated with OH groups), the reaction goes through a different path (see Figure 6). First, as the  $\text{CO}_2$  molecule impinges on the surface, the

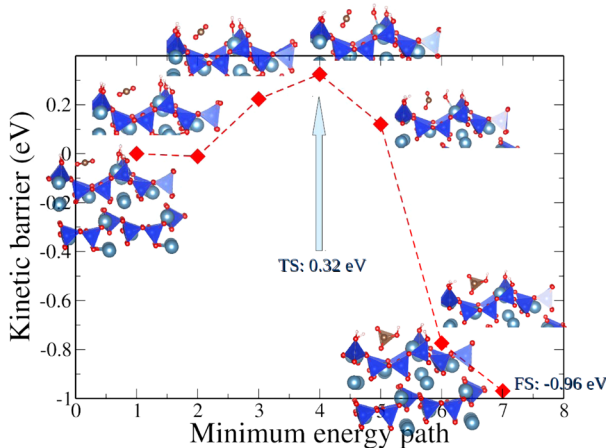


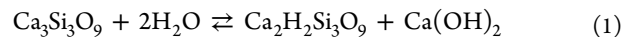
**Figure 6.** Minimum energy path of  $\text{CO}_2$  reacting with  $\text{Wol}(001)$  covered by a full monolayer of water. Deep blue tetrahedra represent Si atoms; red, O; light blue, Ca; white, H; and brown spheres, C atoms, respectively.

physisorption energy is slightly larger than that for the oxygen-terminated,  $\text{H}_2\text{O}$ -free  $\text{Wol}(001)$  surface,  $-0.13$  eV. Second, one of the Si–OH groups tilts to form a hydrogen bridge bond with the  $\text{CO}_2$  molecule (see intermediate configurations of the reaction path shown in Figure 6), in such a way that the  $\text{CO}_2$  rapidly loses its linear configuration to adopt a planar, 2D-like structure. The difference now is that the remaining Si–OH surface bonds act as blocking structures, preventing the spontaneous carbonate formation due to the impossibility of forming additional hydrogen bonds. As shown in Figure 6, in the second half of the reaction, the OH– $\text{CO}_2$  bridge structure etches one of the OH–Ca groups of the surface (a much more energetically favorable process), thus forming a  $\text{CO}_2\text{H}^-$ -structure with a Ca–O bond distance of 2.41 Å, slightly smaller than the previous case. The reaction is slightly exothermic (0.969 eV), and although it needs to overcome a

small kinetic barrier of 0.32 eV, it is not a spontaneous process; i.e., during the simulation time, ab initio MD does not show the carbonate formation from the  $\text{Wol}(001)$  surface at room temperature.

Apart from the  $\text{CO}_2$  adsorption on the valley formed by the O(H) tetrahedra, we also investigated other possible adsorption pathways. For instance, adsorption between the OH groups, in the terrace formed by the O(H) tetrahedra or directly chemisorbed in the valley (without Ca etching). All of them resulted in spontaneous, exothermic reactions but with a lower reaction energy ( $-0.52$ ,  $-0.24$ , and  $-0.14$  eV, respectively).

**C.  $\text{CO}_2$  Reacting with  $\text{Wol}(001)$  Covered by More Than One Monolayer of  $\text{H}_2\text{O}$ .** It appears reasonable to briefly review the most important chemical steps at the  $\text{H}_2\text{O}/\text{Wol}(001)$  interface. In the presence of water, a MPER is happening and leading the surface to a nonstoichiometric thermodynamic ground state in equilibrium with a  $\text{Ca}(\text{OH})_2$  solution:



This process is very fast, meaning that the reaction with  $\text{CO}_2$  can take place inside the solution and  $\text{CaCO}_3$  would fall down on the surface. Oelkers et al. investigated the metal–proton exchange reaction on different minerals and concluded that the number of protons consumed by each exchange reaction is mineral-specific.<sup>15,16</sup>

At the  $\text{H}_2\text{O}/\text{Wol}(001)$  interface, we can describe the carbonation reaction inside the solution as depicted in Figure 7. Water molecules of the hydration shell are cut out of the

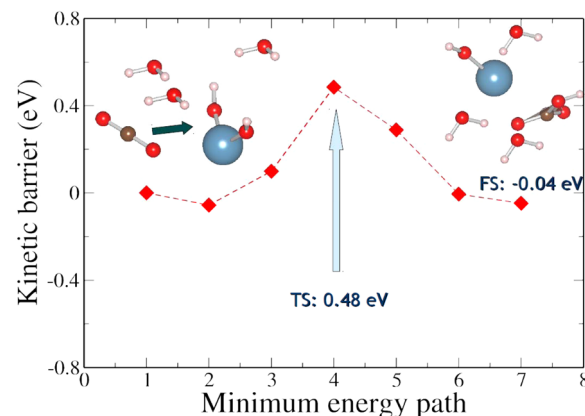


**Figure 7.** Cluster model of the minimum energy path of  $\text{CO}_2$  reacting with  $\text{Wol}(001)$  covered by more than one monolayer of water. Light blue spheres represent Ca atoms; red, O; white, H; and brown spheres, C atoms, respectively.

images to emphasize the low-energy reaction part of the  $\text{CO}_2$  with  $\text{Ca}(\text{OH})_2$ . First, as the  $\text{CO}_2$  molecule approaches the  $\text{Ca}(\text{OH})_2$  in our cluster model, there is a weak physisorption energy of  $-0.05$  eV (half of the obtained value for the Si–OH-terminated surface). Second, the OH groups tilt to form an oxygen bridge bond with the  $\text{CO}_2$  molecule (similarly to the effect shown in Figure 6) and, finally the carbonate  $\text{CO}_3^{2-}$  is formed by detaching one of the OH groups from the Ca. As shown in Figure 7, this is a slightly exothermic process (the reaction energy is only 0.04 eV) with a kinetic barrier larger than that of the Si–OH-terminated surface (cf. 0.48 vs 0.36 eV, see Figures 2 and 3). Considering that the solubility product of

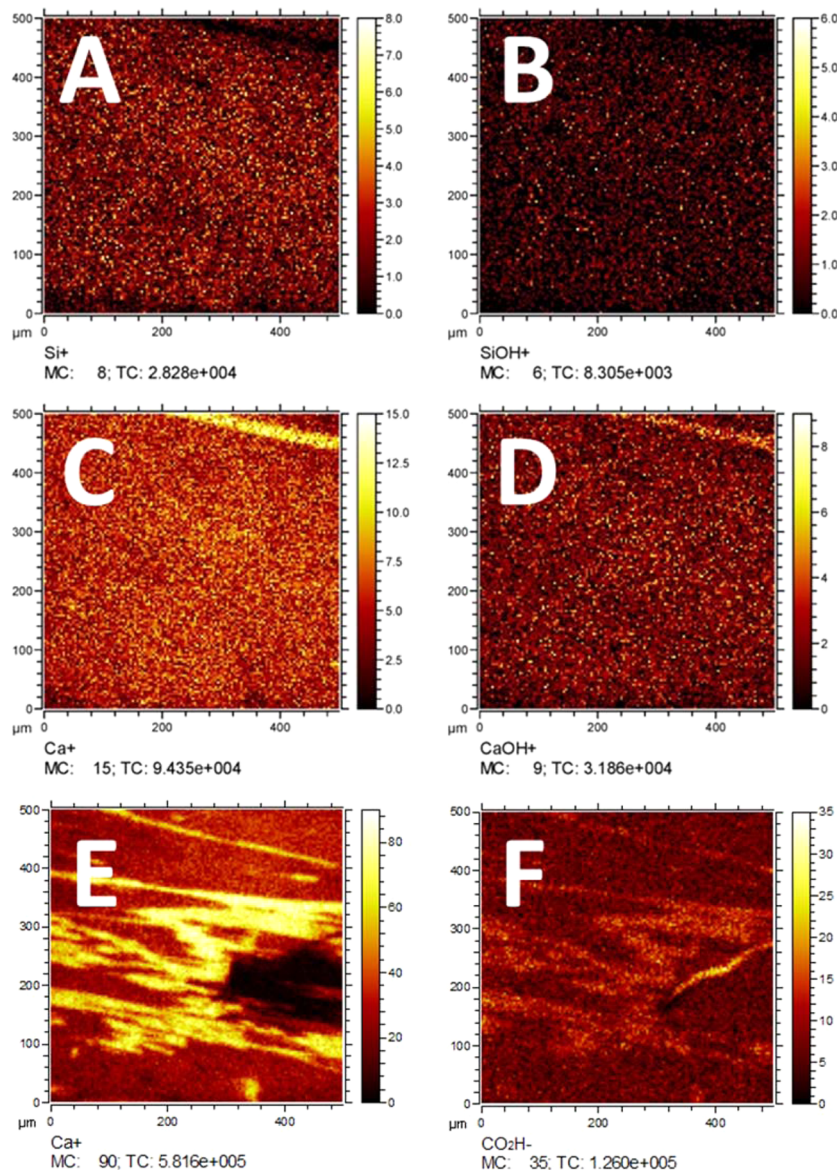


**Figure 8.**  $500 \times 500 \mu\text{m}$  ToF-SIMS mappings of the wollastonite surface. (A)–(D) show results of the wollastonite surface after sputtering the surface. A homogeneous distribution of Ca, seen in (C), can be found. After exposure to air for 24 h, the distribution of Ca has changed into an inhomogeneous distribution, seen in (E), and is directly correlated to the distribution of carbonates, seen in (F).

$\text{CaCO}_3$  is 103 times smaller than the one for  $\text{Ca}(\text{OH})_2$ , the final step of the carbonation has to end on the surface again.

#### 4. DISCUSSION

Among the different reaction paths investigated, we find a strong influence of the chemical potential of water on the kinetics of the carbonation of wollastonite.

**A. Experimental Validation of the Calculations.** The  $\text{H}_2\text{O}$ -free Wol(001) would be a scenario of UHV studies. Bebensee et al. found CaO surfaces to be very reactive regarding carbonate formation.<sup>17</sup> In an interesting study, impinging  $\text{CO}_2$  molecules form  $\text{CO}_3^{2-}$  complexes with surface oxygen atoms. This effect is very similar to the  $\text{CO}_3^{2-}$  formation on  $\text{CaSiO}_3$  films as described in section 3A. Furthermore, they find the dry carbonation to be fast and with a self-limiting character after one monolayer has formed.

In Figure 8,  $500 \times 500 \mu\text{m}$  ToF-SIMS mappings of the wollastonite surface are depicted. (A)–(D) show representative

results of the Wol(001) after sputtering the surface. Sputtering was performed with an argon ion beam energy of 2 keV on a  $2 \times 2 \text{ mm}$  spot. In this state, several considerations are in order. First, Ca and Si are distributed homogeneously over the surface. Second, we can confirm a coexistence of  $\text{Ca}-\text{OH}$  and  $\text{Si}-\text{OH}$  groups which are also homogeneously distributed.<sup>6</sup> After exposure to air for 24 h, the distribution of Ca has changed into an inhomogeneous one, as can be seen in Figure 8E, and is directly correlated to the distribution of carbonates, shown in Figure 8F. The humidity of the air (>30%) combined with earlier thermodynamic studies now allows one to conclude that the mechanism of  $\text{CO}_2$  reacting with Wol(001) covered by more than one monolayer of  $\text{H}_2\text{O}$  is the correct one to describe these highly interesting phenomena. It is the only way to explain (1) heterogeneous distribution of carbonates on the surface and (2) a coverage partially higher/lower than one monolayer.

**B. Impact of the Results.** In this final part, we will try to investigate experimentally the competition between carbonation and hydration on (1) Wol(001), then compare the results to an investigation on (2) commercial cement, and finally do the same investigation on a self-synthesized (3) ultrathin C–S–H phase. All measurements are going to be made by means of low-energy ion-scattering (LEIS) spectroscopy. Decision for LEIS was made due to its possibility to measure on any surface topography.

In Figure 9 B, depicted as a black line, we have measured the Wol(001) surface directly after the transfer from the

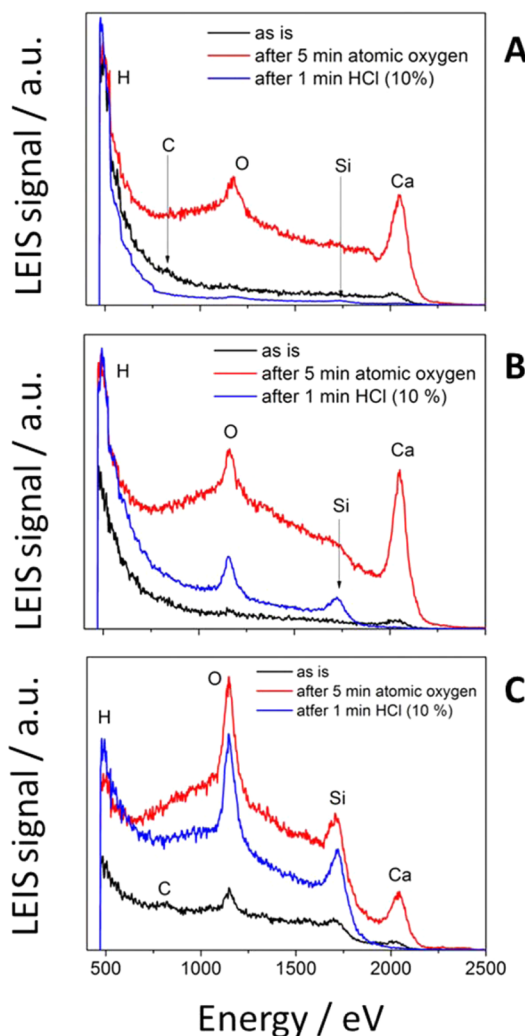


**Figure 9.** Black line shows measurements on the surface (A, concerning commercial cement; B, concerning Wol(001); and C, concerning the ultrathin C–S–H layer) directly after the transfer from the atmosphere. Five minutes of atomic oxygen flux were applied to remove most of the organic components. The red line depicts the consequent measurements. Finally, HCl was exposed to the surfaces for 1 min followed by a last measurement (blue line). In agreement with eq 1, a clear change in the chemical composition can be seen.

atmosphere. As expected, the surface is covered by volatile organic components and hydrogen is the most detected element. Consequently, 5 min of atomic oxygen flux were applied to remove most of the organic components. The red line now depicts a measurement of the Wol(001) surface. Finally, we exposed the Wol(001) surface to hydrochloric acid (HCl) and measured it again. The blue line depicts the

measurements after the exposure to HCl. In agreement with eq 1, a clear change in the chemical composition of the Wol(001) can be seen. The amount of calcium has been reduced while the amount of hydrogen is increased. Furthermore, the amount of silicon is slightly reduced and the oxygen amount seems to stay constant.

In Table 1 we give exact values of the LEIS intensities before and after exposure to HCl. The LEIS intensity is proportional

**Table 1. LEIS Intensities before and after Exposure to HCl**

	Ca/LEIS intensity in counts/nC	Si/LEIS intensity in counts/nC	Ca/Si ratio	O/LEIS intensity in counts/nC
commercial cement	2056	1	2056	1180
commercial cement + HCl	252	242	1	478
Wol(001)	1979	1	1979	658
Wol(001) + HCl	65	614	0.1	762
ultrathin CSH	492	593	0.8	793
ultrathin CSH + HCl	1	777	0	852

to the surface coverage. With the help of these values we can now discuss some discrepancies of the employed model of Wol(001) (Figure 9B), commercial cement (Figure 9A), and the synthesized ultrathin C–S–H phase (Figure 9C). The Ca/Si ratio after exposure to HCl appears most interesting. In the case of the ultrathin C–S–H phase, we propose that the phase was completely consumed during the MPER process; thus, it was no more possible for the resisting system to provide any Ca. In the case of the Wol(001), we propose that the Ca-ion concentration is dependent on the transport mechanism from the bulk material (Ca/Si = 1) to the surface (Ca/Si = 0.1). Since Wol(001) was measured, the transport of the Ca has to run perpendicular to the B-axis. That would for sure slow down the whole process. Finally, the commercial cement has a Ca/Si ratio in the bulk phase of 1.8 and at the surface after exposure to HCl of 1. This is only possible with (1) excellent transport mechanisms in the bulk phase combined with (2) a high reservoir of Ca in the bulk phase.

This work is of broad interest to the material science community because the development of powerful new model systems is one of the most challenging syntheses. In particular, our results have an enormous impact on following research because they show that wollastonite as well as the ultrathin C–S–H layer can be taken as serious model systems regarding the complex cement H<sub>2</sub>O/cement interface.<sup>18,19</sup> The functionalization of concrete surfaces in the presence of H<sub>2</sub>O and CO<sub>2</sub> is of special interest. Building on these results, new strategies regarding surface functionalization can be developed. Finally, the concrete material itself can be further investigated by means of model systems.

## 5. CONCLUSIONS

**A. Dry Carbonation.** The exposure of CaSiO<sub>3</sub> to CO<sub>2</sub> results in a very fast carbonate production. CO<sub>2</sub> reacts with the surface oxygen and forms CO<sub>3</sub><sup>2-</sup> complexes. After a carbonate monolayer has been formed, the reaction comes to a standstill.

**B. Water-Assisted Carbonation.** The reaction is strongly influenced by the chemical potential of water in the environment. The adsorption of CO<sub>2</sub> on CaSiO<sub>3</sub> with a

water monolayer completely changes its mechanism. Due to the metal–proton exchange reaction, the  $\text{Ca}^{2+}$  has been removed partially from the surface and is available for the carbonate reaction in the solution. The thermodynamic ground state of calcium silicate phases in equilibrium with water is reached fast enough to consider it as a realistic scenario to describe the reaction with  $\text{CO}_2$ .

## AUTHOR INFORMATION

### Corresponding Author

\*Karlsruhe Institute of Technology (KIT), Institute of Functional Interfaces (IFG), Hermann-von-Helmholtz-Platz 1, Building 330, 76344 Eggenstein-Leopoldshafen, Germany. Phone: +49 721 608-28223. E-mail: peter.thissen@kit.edu. URL: <http://www.ifg.kit.edu/english/379.php>.

### Notes

The authors declare no competing financial interest.

## ACKNOWLEDGMENTS

The results presented in this paper have been gained within the DFG-funded project TH 1566/3-1. R.L. and K.C. are supported by Global Frontier R&D Program on Center for Multiscale Energy Systems (National Research Foundation for Korea). The authors acknowledge the Texas Advanced Computing Center (TACC) for computational resources.

## REFERENCES

- (1) Stocker, T. F.; Qin, D.; Plattner, G.-K.; Tignor, M.; Allen, S. K.; Boschung, J.; Nauels, A.; Xia, Y.; Bex, V.; Midgley, P. M., Eds. *IPCC, 2013: Climate Change 2013: The Physical Science Basis. Contribution of Working Group I to the Fifth Assessment Report of the Intergovernmental Panel on Climate Change*; Cambridge University Press: Cambridge, U.K., 1535 pp.
- (2) Durgun, E.; Manzano, H.; Pellenq, R. J. M.; Grossman, J. C. Understanding and Controlling the Reactivity of the Calcium Silicate phases from First Principles. *Chem. Mater.* **2012**, *24*, 1262–1267.
- (3) Montes-Hernandez, G.; Pommerol, A.; Renard, F.; Beck, P.; Quirico, E.; Brissaud, O. In Situ Kinetic Measurements of Gas-Solid Carbonation of  $\text{Ca}(\text{OH})_2$  by Using an Infrared Microscope Coupled to a Reaction Cell. *Chem. Eng. J.* **2010**, *161*, 250–256.
- (4) Funk, A.; Trettin, H. F. R. DFT Study on the Effect of Water on the Carbonation of Portlandite. *Ind. Eng. Chem. Res.* **2013**, *52*, 2168–2173.
- (5) Black, L.; Breen, C.; Yarwood, J.; Garbev, K.; Stemmermann, P.; Gasharova, B. Structural Features of C-S-H(I) and its Carbonation in Air - A Raman Spectroscopic Study. Part II: Carbonated Phases. *J. Am. Ceram. Soc.* **2007**, *90*, 908–917.
- (6) Sanna, S.; Schmidt, W. G.; Thissen, P. Formation of Hydroxyl Groups at Calcium-Silicate-Hydrate (C-S-H): Coexistence of  $\text{Ca-OH}$  and  $\text{Si-OH}$  on Wollastonite(001). *J. Phys. Chem. C* **2014**, *118*, 8007–8013.
- (7) Kresse, G.; Hafner, J. Ab Initio Molecular Dynamics for Liquid Metals. *Phys. Rev. B* **1993**, *47*, 558–561.
- (8) Kresse, G.; Furthmuller, J. Efficient Iterative Schemes for Ab Initio Total-Energy Calculations Using a Plane-Wave Basis Set. *Phys. Rev. B* **1996**, *54*, 11169–11186.
- (9) Kresse, G.; Joubert, D. From Ultrasoft Pseudopotentials to the Projector Augmented-Wave Method. *Phys. Rev. B* **1999**, *59*, 1758–1775.
- (10) Blochl, P. E.; Jepsen, O.; Andersen, O. K. Improved Tetrahedron Method For Brillouin-Zone Integrations. *Phys. Rev. B* **1994**, *49*, 16223–16233.
- (11) Perdew, J. P.; Burke, K.; Ernzerhof, M. Generalized Gradient Approximation Made Simple. *Phys. Rev. Lett.* **1997**, *78*, 1396–1396.
- (12) Henkelman, G.; Jonsson, H. Improved Tangent Estimate in the Nudged Elastic Band Method for Finding Minimum Energy Paths and Saddle Points. *J. Chem. Phys.* **2000**, *113*, 9978–9985.
- (13) Henkelman, G.; Uberuaga, B. P.; Jonsson, H. A Climbing Image Nudged Elastic Band Method for Finding Saddle Points and Minimum Energy Paths. *J. Chem. Phys.* **2000**, *113*, 9901–9904.
- (14) Ebbert, C.; Grundmeier, G.; Buitkamp, N.; Kroeger, A.; Messerschmidt, F.; Thissen, P. Toward a Microscopic Understanding of the Calcium-Silicate-Hydrates/Water Interface. *Appl. Surf. Sci.* **2014**, *290*, 207–214.
- (15) Oelkers, E. H.; Golubev, S. V.; Chairat, C.; Pokrovsky, O. S.; Schott, J. The Surface Chemistry of Multi-Oxide Silicates. *Geochim. Cosmochim. Acta* **2009**, *73*, 4617–4634.
- (16) Casey, W. H.; Westrich, H. R.; Banfield, J. F.; Ferruzzi, G.; Arnold, G. W. Leaching and Reconstruction at the Surfaces of Dissolving Chain-Silicate Minerals. *Nature* **1993**, *366*, 253–256.
- (17) Voigts, F.; Bebensee, F.; Dahle, S.; Volgmann, K.; Maus-Friedrichs, W. The Adsorption of  $\text{CO}_2$  and CO on Ca and  $\text{CaO}$  Films Studied with MIES, UPS and XPS. *Surf. Sci.* **2009**, *603*, 40–49.
- (18) Garrault, S.; Behr, T.; Nonat, A. Formation of the C-S-H Layer During Early Hydration of Tricalcium Silicate Grains with Different Sizes. *J. Phys. Chem. B* **2006**, *110*, 270–275.
- (19) Garrault, S.; Finot, E.; Lesniewska, E.; Nonat, A. Study of C-S-H Growth on C3S Surface During its Early Hydration. *Mater. Struct.* **2005**, *38*, 435–442.